Available online at www.sciencedirect.com

ScienceDirect

Energy Procedia 117 (2017) 835–846

Energy Procedia

www.elsevier.com/locate/procedia

1st International Conference on Power Engineering, Computing and CONtrol, PECCON-2017, 2-4 March 2017, VIT University, Chennai Campus

Small Signal Modeling of a DC-DC Type Double Boost Converter Integrated With SEPIC Converter Using State Space Averaging Approach

Kanimozhi.G,Meenakshi.J,Sreedevi.VT*

VIT University,vandalur-kelambakkam Road,chennai-600127,India

Abstract

This study presents a detailed small signal analysis of a DC-DC type double boost converter integrated with SEPIC converter. The integrated converter has the features of the conventional boost and SEPIC converters, such as continuous input current, low input current ripple with extended step up capability. The converter consists of seven dynamic elements and hence it would be interesting to study the small-signal model of the converter. State-space averaging technique is used to derive the small signal model. The duty ratio control to output voltage transfer function is derived. A 50W prototype of the integrated double boost SEPIC converter is implemented using PIC 16F887 microcontroller, operating in continuous conduction mode. The measured results on the prototype verify the theoretical analysis**.**

Peer-review under responsibility of the scientific committee of the 1st International Conference on Power Engineering, Computing and CONtrol.

Keywords: small signal modeling;SEPIC converter;state space averaging;

1. Introduction

Renewable energy sources attract popularity to meet the increased energy demand worldwide. Renewable energy sources like photovoltaic (PV) cells and fuel cells produce a low dc output voltage. A high step up dc-dc power converter is necessary to convert the low dc output voltage to a boosted dc voltage suitable for an inverter

*Sreedevi.VT. Tel.: +91 9444300126
E-mail address: sreedevi.vt@vit.ac.in

1876-6102
Peer-review under responsibility of the scientific committee of the 1st International Conference on Power Engineering, Computing and CONtrol.
10.1016/j.egypro.2017.05.201

to feed ac load.

Traditional dc –dc converter topologies are unable to provide a gain greater than 6 [1-3].Cascaded boost converters with a single switch provide high output voltage without extreme duty cycle operation of the switch [4-5]. But they are less efficient because the output of the first stage is the input of the second stage and cascading increases number of components of the converter. Converters employing coupled inductors provide high step up [6-9], however, large input current ripple is a disadvantage. Boost converters modified with voltage multiplier cells with single switch are another solution for high output voltage [10-11], but for higher power, the current stress of the switch is an issue. Interleaving technique [11-12] is introduced to reduce input current ripple, but it suffers from high gain, while achieving less input current ripple.

Many integrated topologies by combining the advantages of simple, traditional converters are proposed to obtain high gain [13-15]. A buck boost fly-back integrated converter is proposed to achieve a boosted voltage from a fuel cell for grid tied applications [13]. A fully-integrated high- conversion-ratio dual-output voltage boost converter for obtaining boosted output from low voltage energy sources is proposed [14]. A soft-switched dual-boost coupled-inductor-based converter by combining of forward and fly-back converter with required high voltage is introduced in [15]. Detailed steady state analysis, principle of operation and design of the above modified converters are explained in the literature. But a small signal modelling approach is essential for closed loop application such as for low voltage energy harvesting from renewable energy sources.

A double boost converter integrated with a SEPIC converter is presented in [16] to boost the fuel cell/PV output voltage. This converter is suitable for fuel cell/ PV applications because it combines the features of conventional boost and SEPIC converter with continuous input current with less ripple content and a better voltage conversion ratio [16]. This work focuses on the small signal modeling and controller design of the double boost converter integrated with SEPIC presented in [16] using a single switch for PV/ fuel cell applications. Small signal modeling for nonlinear pulse width modulated dc-dc converters are a useful tool for controller design and better understanding of the circuit performance [17-19]. A detailed small signal analysis and a closed loop design using a two-loop average current controller is presented for a zero voltage switched two inductor active-clamped current fed isolated DC-DC converters [20]. State space averaging technique is used to derive the small signal model [21-22]. Another study presents a small signal model using signal flow graph and Mason's gain formula for open loop SEPIC converter [23]. State space averaging technique is tedious, when the number of elements of the converter is too many; hence a signal flow graph approach is discussed [24-25].

The topology of double boost converter integrated with SEPIC presented in [16] is shown in Fig. 1. It consists of seven dynamic elements and hence it would be interesting to study the small-signal model of the converter. State-space averaging technique is used to derive the small signal model, though the number of state variables is high. The control to output transfer function is derived. The measured results in a 50W prototype operating in continuous conduction mode are in good agreement with the theoretical predictions. It is verified that the converter is capable of providing continuous input current with reduced ripple with a better voltage conversion ratio than traditional topologies. The remaining part of the paper is organized as follows: Section 2 describes the small signal modelling of the double boost converter integrated with SEPIC. Section 3 discusses the experimental results. Section 4 concludes the paper.

2. **Small Signal Modelling**

The double boost converter integrated with SEPIC converter is shown in Fig.1 [16]. It consists of a switch Q, four diodes,(D_1, D_2, D_3, D_4) two inductors (L_1, L_2) and five capacitors C_1, C_2, C_3, C_4 and C_5. In this section, state-space equations for each mode of operation of the converter are described. Then small signal model is presented based on state-space averaging technique. The averaged state space model can be obtained by computing the required derivatives and output equations separately for the switch Q ON and OFF times, multiplying those equations by the duty ratio (D) and its complement $(1 - D)$ and summing them together.

Analysis of the converter is based on the following assumptions:

- The MOSFET switch and diodes are ideal.
- The capacitors are large enough, thus capacitor voltages are considered constant in one switching period.

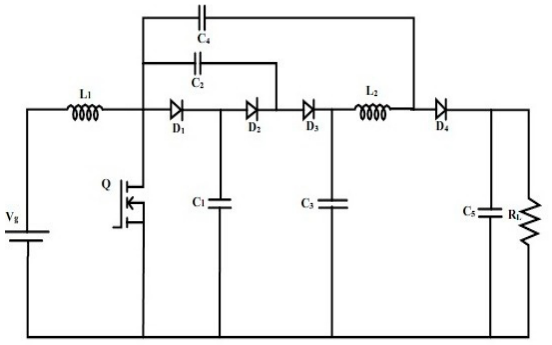

Fig1. Double boost converter integrated with SEPIC converter

The switch Q is operating at a switching frequency $f = \frac{1}{T}$ with duty ratio of the switch is given by $D = \frac{Ton}{T}$, where T_{on} is the ON time of the switch. Operation of the converter is assumed to be in the continuous conduction mode (CCM). The circuit operation is divided into two modes in one switching cycle.

2.1 State Equations for Mode 1

During mode 1, the switch Q is turned on, as shown in Fig. 2.

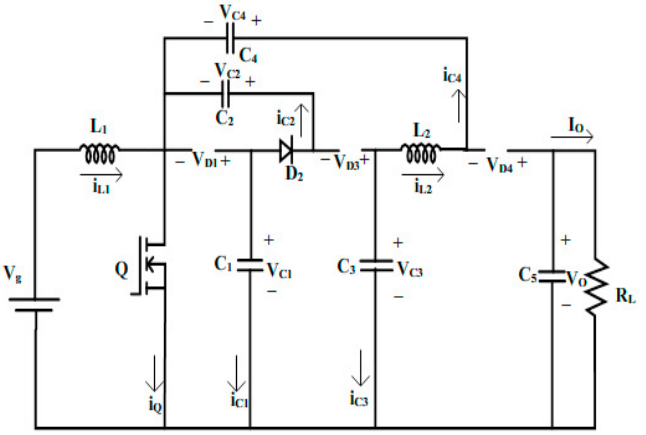

Fig.2. Equivalent circuit for Mode 1.

Diode D_2 is turned on simultaneously when switch Q is on. Diode D_1 is open –circuited by the capacitor voltage V_{C1}.Diodes D_3 and D_4 are reverse biased, since voltages $(V_{C1} - V_{C3})$ and $(V_{C4} - V_o)$ appear across them respectively. The current through L_1 (i_{L1}) increases linearly. In this mode, capacitor C_1 charges capacitor C_2 while capacitor C_4 is being charged by inductor current L_2 (i_{L2}). The voltage across capacitors C_1 and C_2 are equal, while the difference between the capacitor's voltages V_{C3} and V_{C4} is equal to the input voltage, i.e. $V_{C1} = V_{C2}$ (1)

$$V_g = V_{C3} - V_{C4} \quad (2)$$

At the end of this interval, the switch is turned-off initiating the next subinterval. State variables defined for the small signal modeling of the converter are (i) Currents through the boost inductors i_{L1} and i_{L2}. (ii) Voltage across the capacitors C_1, C_2, C_3, C_4, and C_5, i.e, $v_{C1}(t)$, $v_{C2}(t)$, $v_{C3}(t)$, $v_{C4}(t)$ and $v_{C5}(t)$.The state vector is defined as

$$x(t) = [i_{L1}(t)\ i_{L2}(t)\ v_{C1}(t)\ v_{C2}(t)\ v_{C3}(t)\ v_{C4}(t)\ v_{C5}(t)]^T \quad (3)$$

The input voltage is chosen as the input variable so that the input vector is given by

$$u(t) = V_g(t) \quad (4)$$

The state equations for this interval are

$$\dot{i}_{L1} = \frac{V_g(t)}{L_1} \quad (5)$$

$$\dot{i}_{L2} = \frac{(V_{C3}) + (V_{C4})}{L_2} \quad (6)$$

$$\dot{v}_{C1} = \frac{i_{L1}}{C_1} - \frac{i_{L2}}{C_1} \quad (7)$$

$$\dot{v}_{C2} = \frac{i_{L1}}{C_2} - \frac{i_{L2}}{C_2} \quad (8)$$

$$\dot{v}_{C3} = \frac{i_{L2}}{C_3} \quad (9)$$

$$\dot{v}_{C4} = \frac{i_{L2}}{C_4} \quad (10)$$

$$\dot{v}_{C5} = -\frac{V_0}{R_L C_5} \quad (11)$$

The differential equations governing the dynamics of state vector $x(t)$ for switch-ON period can be written in state space form as $\dot{x}(t) = A_1 x(t) + B_1 u(t)$ (12)

where

$$A_1 = \begin{bmatrix} 0 & 0 & 0 & 0 & 0 & 0 & 0 \\ 0 & 0 & 0 & 0 & \frac{1}{L_2} & -\frac{1}{L_2} & 0 \\ \frac{1}{C_1} & -\frac{1}{C_1} & 0 & 0 & 0 & 0 & 0 \\ \frac{1}{C_2} & -\frac{1}{C_2} & 0 & 0 & 0 & 0 & 0 \\ 0 & \frac{1}{C_3} & 0 & 0 & 0 & 0 & 0 \\ 0 & \frac{1}{C_4} & 0 & 0 & 0 & 0 & 0 \\ 0 & 0 & 0 & 0 & 0 & 0 & 0 \end{bmatrix} \quad \text{and} \quad B_1 = \begin{bmatrix} \frac{1}{L_1} \\ 0 \\ 0 \\ 0 \\ 0 \\ 0 \\ 0 \end{bmatrix}$$

respectively. When switch is in ON, output voltage $V_o = V_{C5}$ (13)

and the output vector is $y(t) = C_1 x(t)$ where $C_1 = [0\ \ 0\ \ 0\ \ 0\ \ 0\ \ 0\ \ 1]$ (14)

2.2 State Equations for Mode 2

The equivalent circuit for Mode-2 is given in Fig. 3. Theoretical waveforms of the converter in CCM are given in figure 4. It is seen from Fig. 4 that at t_1, switch Q is off,. Diodes D_1, D_3 and D_4 are forward biased so that input and output inductor currents flow. Diode D_2 is OFF by the capacitor voltage V_{C2}. In this mode, the

inductor currents i_{L1} and i_{L2} reduces in proportion to the voltage $(V_g - V_{C1})$ and $(V_{C3} - V_0)$ respectively. From Fig.3, it is clear that the capacitors C_1 and C_3 are being charged by the currents, $(i_{L1} + i_{C2} + i_{C4})$ and $(i_{D3} - i_{L2})$ respectively. During this mode, the output capacitor C_5 is being charged by the current $(i_{L2} - i_{C4})$.

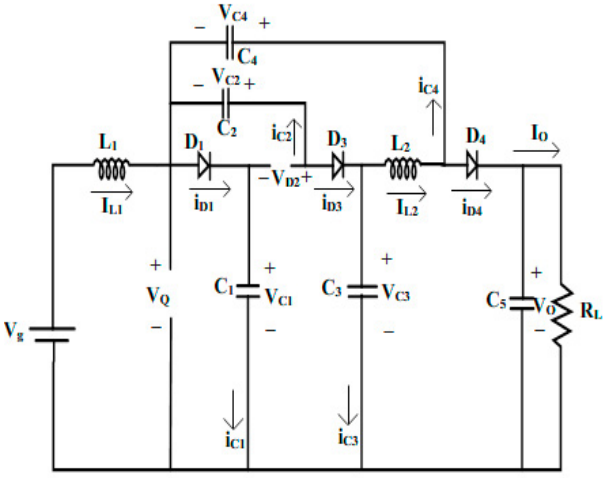

Fig.3. Equivalent circuit for Mode 2.

The output voltage V_o referring to Fig. 3 is expressed as

$$V_0 = V_{C1} + V_{C4} - V_{C2} \tag{15}$$

$$V_{C3} = 2V_{C1} \tag{16}$$

The state equations for mode 2 are

$$\dot{i}_{L1} = \frac{V_g - V_{C1}}{L_1} \tag{17}$$

$$\dot{i}_{L2} = \frac{V_{C2} - V_{C4}}{L_2} \tag{18}$$

$$\dot{V}_{C1} = \frac{i_{L1}}{(C_1 - 2C_3)} + \frac{2i_{L2}}{(C_1 - 2C_3)} + \frac{V_{C2}}{R_L(C_1 - 2C_3)} - \frac{V_{C3}}{R_L(C_1 - 2C_3)} - \frac{V_{C4}}{R_L(C_1 - 2C_3)} \tag{19}$$

$$\dot{V}_{C2} = \frac{2C_3}{C_2(C_1 - 2C_3)} i_{L1} + \frac{(C_1 + 2C_3)}{C_2(C_1 - 2C_3)} i_{L2} + \frac{2C_3}{R_L C_2(C_1 - 2C_3)} V_{C2} - \frac{2C_3}{R_L C_2(C_1 - 2C_3)} V_{C3} - \frac{2C_3}{R_L C_2(C_1 - 2C_3)} V_{C4} \tag{20}$$

$$\dot{V}_{C3} = \frac{2}{(C_1 - 2C_3)} i_{L1} + \frac{4}{(C_1 - 2C_3)} i_{L2} + \frac{2}{R_L(C_1 - 2C_3)} V_{C2} - \frac{2}{R_L(C_1 - 2C_3)} V_{C3} - \frac{2}{R_L(C_1 - 2C_3)} V_{C4} \tag{21}$$

$$\dot{V}_{C4} = \frac{i_{L2}}{C_4} + \frac{V_{C2}}{R_L C_4} - \frac{V_{C3}}{R_L C_4} - \frac{V_{C4}}{R_L C_4} \tag{22}$$

$$\dot{V}_{C5} = \frac{1-C_4}{R_L C_5} V_{C2} - \frac{1-C_4}{R_L C_5} V_{C3} - \frac{1-C_4}{R_L C_5} V_{C4} \tag{23}$$

The state equations for switch OFF duration can be written in state space form as

$$\dot{x}(t) = A_2 x(t) + B_2 u(t) \tag{24}$$

Where matrix A_2 and B_2 are given by

$$A_2 = \begin{bmatrix} 0 & 0 & -\frac{1}{L_1} & 0 & 0 & 0 & 0 \\ 0 & 0 & 0 & 0 & \frac{1}{L_2} & 0 & 0 \\ \frac{1}{(C_1-2C_3)} & \frac{2}{(C_1-2C_3)} & 0 & 0 & 0 & 0 & 0 \\ \frac{2C_3}{C_2(C_1-2C_3)} & \frac{(C_1+2C_3)}{C_2(C_1-2C_3)} & 0 & 0 & 0 & 0 & 0 \\ \frac{2}{(C_1-2C_3)} & \frac{4}{(C_1-2C_3)} & 0 & 0 & 0 & 0 & 0 \\ 0 & \frac{1}{C_4} & 0 & 0 & 0 & 0 & 0 \\ 0 & 0 & 0 & 0 & 0 & 0 & 0 \end{bmatrix} \qquad B_2 = \begin{bmatrix} \frac{1}{L_1} \\ 0 \\ 0 \\ 0 \\ 0 \\ 0 \\ 0 \end{bmatrix}$$

The output matrix is given by

$$Y(t) = C_2 X(t) \quad \text{where} \quad C_2 = \begin{bmatrix} 0 & 0 & 0 & -1 & 1 & 1 & 0 \end{bmatrix} \tag{25}$$

The output voltage gain K of the double boost converter integrated with SEPIC is given by equation (26) [16].

$$K = \frac{(2+D)}{(1-D)} \tag{26}$$

Therefore it is suitable for harvesting energy from low voltage renewable energy sources.

2.3. State space averaging approach:

The state space averaging approach is used to obtain the small-signal model. Applying the averaging concept to the state-space models given in equations (12) and (24), the state space average model of converter is determined as

$$\dot{x}(t) = \left[A_1 D + A_2 D'\right] x(t) + \left[B_1 D + B_2 D'\right] u(t) \tag{27}$$

where $D' = 1 - D$. (28)

A general description of the averaged state space model can be given by

$$\dot{x}(t) = Ax(t) + Bu(t) \tag{29}$$

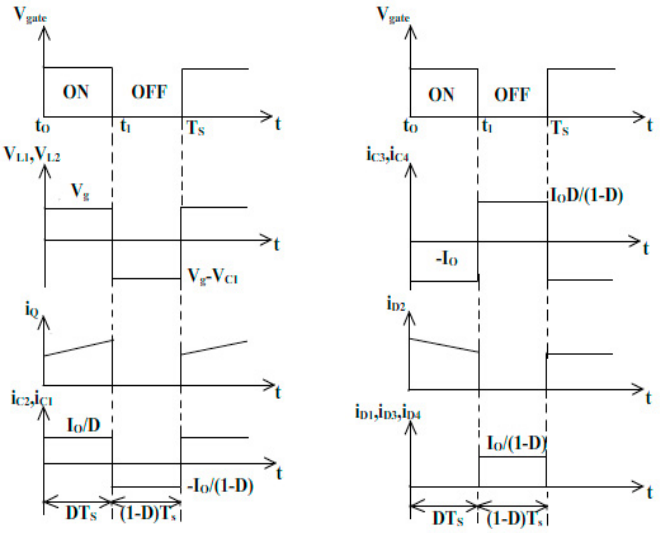

Fig. 4. Theoretical waveforms of the converter.

where $A =$

$$\begin{bmatrix} 0 & 0 & \frac{-(1-D)}{L_1} & 0 & 0 & 0 & 0 \\ 0 & 0 & 0 & \frac{(1-D)}{L_2} & 0 & \frac{-(1-D)}{L_2} & 0 \\ \frac{1}{C_1} & \frac{C_1-3D}{C_1-2C_3} & 0 & \frac{(1-D)}{R_L(C_1-2C_3)} & -\frac{(1-D)}{R_L(C_1-2C_3)} & -\frac{(1-D)}{R_L(C_1-2C_3)} & 0 \\ \frac{[C_1C_2D+2C_2C_3(1-2D)]}{C_2(C_1-2C_3)} & \frac{[C_1C_2(1-2D)+2C_2C_3]}{C_2(C_1-2C_3)} & 0 & \frac{2C_3(1-D)}{R_LC_2(C_1-2C_3)} & \frac{-2C_3(1-D)}{R_LC_2(C_1-2C_3)} & \frac{-2C_3(1-D)}{R_LC_2(C_1-2C_3)} & 0 \\ \frac{2(1-D)}{C_1-2C_3} & \frac{[C_1D+2C_3(2-3D)]}{C_3(C_1-2C_3)} & 0 & \frac{2(1-D)}{R_L(C_1-2C_3)} & \frac{-2(1-D)}{R_L(C_1-2C_3)} & \frac{-2(1-D)}{R_L(C_1-2C_3)} & 0 \\ 0 & \frac{1}{C_4} & 0 & \frac{(1-D)}{R_LC_4} & \frac{-(1-D)}{R_LC_4} & \frac{-(1-D)}{R_LC_4} & 0 \\ 0 & 0 & 0 & \frac{(1-C_4)(1-D)}{R_LC_5} & \frac{-(1-C_4)(1-D)}{R_LC_5} & \frac{-(1-C_4)(1-D)}{R_LC_5} & 0 \end{bmatrix}$$

$$B = \begin{bmatrix} \frac{1}{L_1} \\ \frac{D}{L_2} \\ 0 \\ 0 \\ 0 \\ 0 \\ 0 \end{bmatrix}$$

The next step in the modeling of the converter is the introduction of small ac signals in the average value of the variables, aiming to analyze the behaviour of the converter subjected to these perturbations. Thus, the average variables become approximation of the system is obtained. The dc terms are neglected since they are already represented by the steady state model. Hence the small signal analysis is focused only on the ac behaviour.

$$x(t) = X + \tilde{x}(t) \tag{30}$$

$$d(t) = D + \tilde{d} \tag{31}$$

$$V_g(t) = V_g + \tilde{v}_g(t) \tag{32}$$

$$\begin{bmatrix} \dot{i}_{L1} \\ \dot{i}_{L2} \\ \dot{V}_{C1} \\ \dot{V}_{C2} \\ \dot{V}_{C3} \\ \dot{V}_{C4} \\ \dot{V}_{C5} \end{bmatrix} = \begin{bmatrix} 0 & 0 & \frac{-(1-D)}{L_1} & 0 & 0 & 0 & 0 \\ 0 & 0 & 0 & \frac{(1-D)}{L_2} & 0 & \frac{-(1-D)}{L_2} & 0 \\ \frac{1}{C_1} & \frac{C_1-3D}{C_1-2C_3} & 0 & \frac{(1-D)}{R_L(C_1-2C_3)} & -\frac{(1-D)}{R_L(C_1-2C_3)} & -\frac{(1-D)}{R_L(C_1-2C_3)} & 0 \\ \frac{[C_1C_2D+2C_2C_3(1-2D)]}{C_2(C_1-2C_3)} & \frac{[C_1C_2(1-2D)+2C_2C_3]}{C_2(C_1-2C_3)} & 0 & \frac{2C_3(1-D)}{R_LC_2(C_1-2C_3)} & \frac{-2C_3(1-D)}{R_LC_2(C_1-2C_3)} & \frac{-2C_3(1-D)}{R_LC_2(C_1-2C_3)} & 0 \\ \frac{2(1-D)}{C_1-2C_3} & \frac{[C_1D+2C_3(2-3D)]}{C_3(C_1-2C_3)} & 0 & \frac{2(1-D)}{R_L(C_1-2C_3)} & \frac{-2(1-D)}{R_L(C_1-2C_3)} & \frac{-2(1-D)}{R_L(C_1-2C_3)} & 0 \\ 0 & \frac{1}{C_4} & 0 & \frac{(1-D)}{R_LC_4} & \frac{-(1-D)}{R_LC_4} & \frac{-(1-D)}{R_LC_4} & 0 \\ 0 & 0 & 0 & \frac{(1-C_4)(1-D)}{R_LC_5} & \frac{-(1-C_4)(1-D)}{R_LC_5} & \frac{-(1-C_4)(1-D)}{R_LC_5} & 0 \end{bmatrix} \begin{bmatrix} i_{L1} \\ i_{L2} \\ V_{C1} \\ V_{C2} \\ V_{C3} \\ V_{C4} \\ V_{C5} \end{bmatrix}$$

$$+ \begin{bmatrix} \frac{E}{L_1(1-D)} & \frac{1}{L_1} \\ \frac{E}{L_2(1-D)} & \frac{1}{L_2} \\ \frac{-3E}{C_1-2C_3(1-D)} & 0 \\ \frac{(-C_1C_2-4C_2C_3)E}{C_2(C_1-2C_3)(1-D)} & 0 \\ \frac{(-2+C_1-6C_3)2E}{1-D} & 0 \\ \frac{1}{R_LC_4} & 0 \\ \frac{C_4-1}{R_LC_5} & 0 \end{bmatrix} \begin{bmatrix} d \\ e \end{bmatrix} \tag{33}$$

The derived small signal model leads the control to output voltage transfer function. By using Laplace transform in equation (33), and making the perturbations of the input voltage variations be zero, the transfer function from the duty cycle to the output voltage is derived.

The design equations for the converter elements in order to operate the converter in continuous conduction mode are explained from equations (37) to (42). The design of the inductances L_1, L_2 is same of the classical boost converter.

$$L_1 = \frac{(V_g * D)}{(\Delta I_{L1} * f_s)} \tag{34}$$

Where Δi_{L1}=current ripple through L_1; Δi_{L2}=current ripple through L_2; ΔV_c= capacitor voltage ripple

P_o=output power.

$$C_1, C_2 \geq \frac{P_o}{(V_{C1}^2 * f_s)} \tag{38}$$

$$C_3 = \frac{(\Delta I_{L2} * D)}{(\Delta V_C * f_s)} \tag{35}$$

$$C_4 = \frac{(\Delta I_{L2} * D)}{(\Delta V_C * f_s)} \tag{36}$$

$$C_5 = \frac{D}{(2 * f_s * R_L)} \tag{37}$$

$$L_2 = \frac{(V_g * D)}{(\Delta I_{L2} * f_s)} \tag{38}$$

In this work, Δi_{L1} and Δi_{L2} are taken as 0.96 A and 1.066 A respectively. The capacitor voltage ripple is 1.6 V. To verify the above theoretical analysis, simulation results are carried out for the converter using MATLAB/SIMULINK [26] according to the converter specifications mentioned in Table-1.

Table-1 Specifications of the Converter

Capacitors, C_1, C_2, C_3	10μF
Capacitor, C_4, C_5	1000μF
Inductor, L_1	330μH
Inductor, L_2	660μH
Load Resistor, R_L	128Ω
Diodes D_1, D_2, D_3 and D_4	MUR860
MOSFET	IRF250N
MOSFET driver	TLP250
Voltage sensor	LV25P

The transfer function of the system is obtained, as given in equation (39), by substituting the above parameters mentioned in Table-1.

$$Gvd(s) = \frac{4.359*10^{14}s^6 - 4.36*10^{14}s^5 - 3.409*10^{12}s^4 + 1.102*10^{14}s^3 + 4.691s^2 + 1.2*10^{10}s - 3.902*10^{-5}}{s^7 - 1.011*10^{10}s^6 + 76376s^5 + 6.545*10^{13}s^4 + 2.424*10^{8}s^3 + 4.04*10^{4}s^2 + 375s + 125} \tag{39}$$

The pole–zero plot of the above transfer function is shown in Fig.5 which has two zeros on the right half sides of the s-plane and hence it is a non minimum phase system.

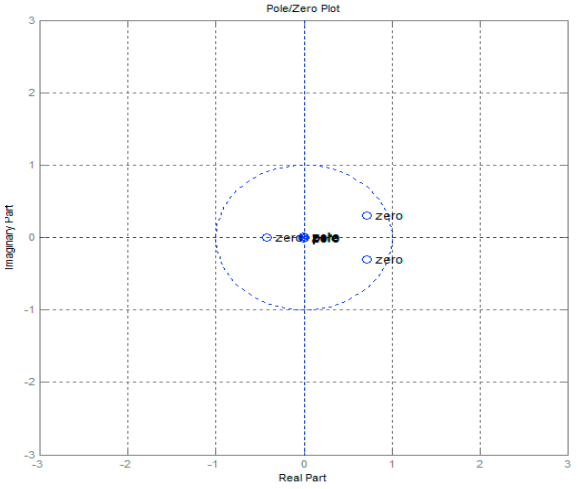

Fig.5: The pole-zero plot.

3 Experimental Results

To verify the performance of the switching converter, a prototype delivering an output power of 50 W has been fabricated with the specifications given in Table-1. The prototype is tested for open loop and closed loop for an input voltage of 20V with a duty ratio of 40%. The converter operates with a switching frequency of 25 kHz. Diodes utilized in the converter circuit are MUR860. It has the features of low leakage current and low forward voltage drop with low switching losses. The MOSFET switch for the converter utilizes IRF250N. TLP250 driver IC is used for stepping up the voltage level necessary for triggering the MOSFET. The PIC16F887 is a 40-pin integrated circuit (IC) and houses mainly 256 bytes of EEPROM data memory, 2 Comparators, 14 channels of 10-bit Analog-to-Digital (A/D) converter, PWM generator, synchronous serial port, and Universal Asynchronous Receiver Transmitter (USART)[26]. The performance of the converter is verified in both open loop condition. Converter waveforms in open loop are presented in Fig. 6 which shows the pulses generated to the switch Q, inductor current ripples, output voltage, output current and voltage stress across the switch Q. The current through the inductors clearly demonstrate CCM operation. The output voltage is 80V which satisfies the gain equation (26) for a duty ratio of 40%. It can be seen that the output current is ripple free from Fig. 6(c) and it makes the converter suitable for PV and fuel cell applications. The voltage stress across the switch Q is lesser than that of a classical double boost and SEPIC converter [16]. The voltage stress across the switch is shown in Fig. 6 (d). It is seen from Fig.6 (d) that $V_{stress,Q} = V_{C1}$ = 33.3 V.

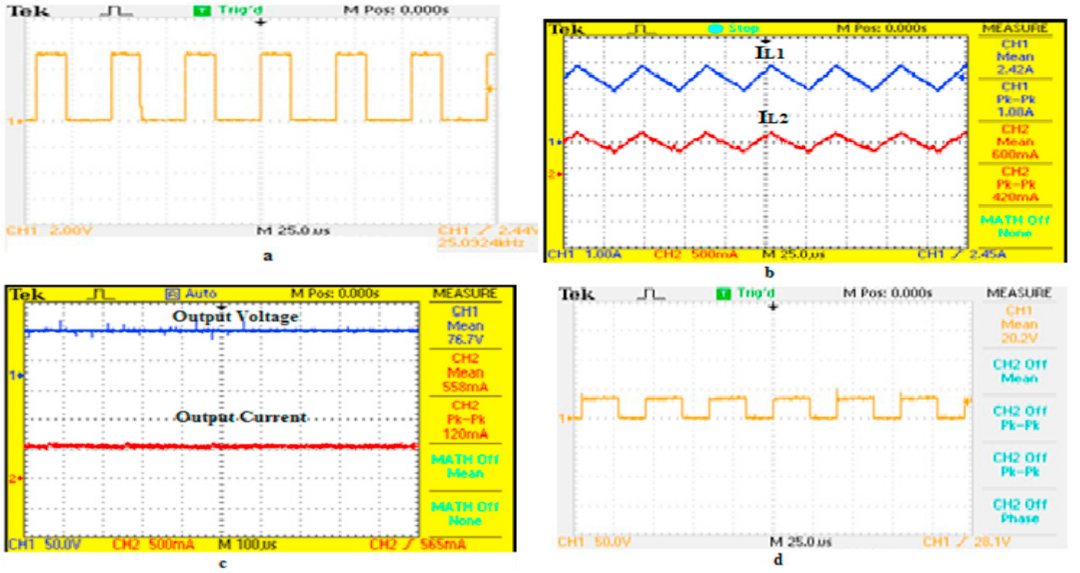

Fig 6. Waveforms in open loop (a) pulses generated to switch Q (b) ripple current through inductors (c) Output voltage and output current (d) voltage across the switch Q.

V_{C1}, V_{C2}, V_{C3} and V_{C4} are shown in Fig.7. These capacitor voltages agree with the steady state equations (1), (2), (13), (15) and (16) described in section 2. The voltages across the diodes D_1, D_2, D_3 and D_4 can be determined by equations (47) to (50) and are shown in Fig.8. These values are in good agreement with the theoretical calculations as given by equations (40) to (43).

$$V_{D1} = D * V_{C1} \tag{40}$$

$$V_{D2} = (1-D) * V_{C2} \tag{41}$$

$$V_{D3} = D * (V_{C3} - V_{C1}) \tag{42}$$

$$V_{D4} = D * (V_O - V_{C4}) \tag{43}$$

Fig. 7. The voltage across the capacitances (a) V_{C1} (b) V_{C2} (c) V_{C3} (d) V_{C4}

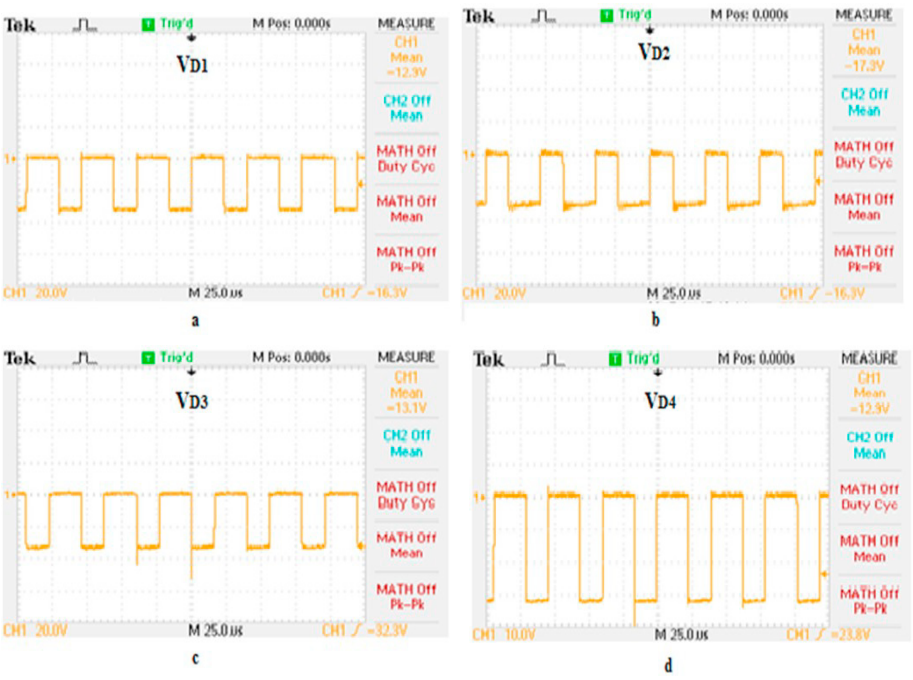

Fig. 8. Voltage stress across the diodes (a) D_1 (b) D_2 (c) D_3 (d) D_4

3 Conclusion

This paper presents small signal modeling for a dc-dc type double boost converter integrated with SEPIC converter which is useful for controller design for PV and fuel cell applications. State-space averaging technique is used to derive the small signal model. The duty ratio control to output voltage transfer function is derived. A 50W prototype of the converter is implemented using PIC 16F887 microcontroller, operating in continuous conduction mode. The measured results on the prototype verify the theoretical analysis.

References

[1] Shahin A, Hinaje M, Martin J.P, Pierfederici,S, Rael S, Davat B. High Voltage Ratio DC-DC Converter for Fuel-Cell Applications. IEEE T on Ind Electron 2010;57:3944-3955.
[2] M. H. Todorovic, L. Palma, P. N. Enjeti. Design of a wide input range dc–dc converter with a robust power control scheme suitable for fuel-cell power converters. IEEE T on Ind Electro 2008;55: 1247–1255.
[3] Park, K.B, Moon, G.W, Youn, M.J. Non isolated high step-up stacked converter based on boost-integrated isolated converter. IEEE T on Power Electr 2011;26:577–587.
[4] Haroun, R, Cid-Pastor, A, El Aroudi, A.. Martínez-Salamero, L.Synthesis of canonical elements for power processing in DC distribution systems using cascaded converters and sliding-mode control IEEE T on Power Electr 2014;29:1366-1381.
[5] Haroun, R, El Aroudi, A, Cid-Pastor, A, et al. Impedance matching in photovoltaic systems using cascaded boost converters and sliding-mode control, IEEE T on Power Electr 2015;30: 3185–3199.
[6] Yang, L.S, Liang, T.J, Lee, H.C,Chen, J.F, Novel high step-up DC– DC converter with coupled-inductor and voltage-doubler circuits. IEEE T on Ind Electron 2011; 58: 4196–4206.
[7] Wu, T.F, Lai, Y.S, Hung, J.C,Chen, Y.M, "Boost converter with coupled inductors and buck-boost type of active clamp. IEEE T on Ind Electron 2008;55:154 – 162.
[8] Hu, X, Gong C.A high voltage gain DC-DC converter integrating coupled inductor and diode capacitor techniques. IEEE T on Power Electr 2014:29: 789-800.
[9] Changchien, S.-K, Liang, T.-J, Chen, J.-F, et al.Step-up DC–DC converter by coupled inductor and voltage-lift technique. IET Power Electron 2010;3: 369–378.
[10] Young, C.M, Chen, M.H, Chang, T.A, Ko, C.C. Jen, K.K. Cascaded voltage multiplier applied to transformer less high step-up DC-DC converter. IEEE T on Ind Electron 2013; 60:523-537.
[11] Tseng, K.C, Huang, C.C. High step-up high-efficiency interleaved converter with voltage multiplier module for renewable energy system IEEE T on Ind Electron 2014;61:1311-1319.
[12] Li, W, Xiang, X, Li, C, Li, W, and He, X, "Interleaved high step-up ZVT converter with built-in transformer voltage doubler cell for distributed PV generation system," IEEE T on Ind Electron 2013;28:300-313.
[13] Chih-Lung Shen, Po-Chieh Chiu. Buck-boost-flyback integrated converter with single switch to achieve high voltage gain for PV or fuel-cell applications. IET Power Electronics 2016; 9:1-10.
[14] Toshihiro Ozaki, Tetsuya Hirose, Hiroki Asano,Nobutaka Kuroki, Masahiro Numa. Fully-Integrated High-Conversion-Ratio Dual-Output Voltage Boost Converter with MPPT for Low-Voltage Energy Harvesting. IEEE J Solid-St Circ 2016:1-10.
[15] Hadi Moradi Sizkoohi, Jafar Milimonfared, Meghdad Taheri, Sina Salehi. High step-up soft-switched dual-boost coupled-inductor-based converter integrating multipurpose coupled inductors with capacitor-diode stages. IET Power Electronic 2015;8: 1786 – 1797.
[16] Sabzali,A.J, Ismail, E.H, Behbehani, H.M,High voltage step-up integrated double Boost-Sepic DC-DC converter for fuel-cell and photovoltaic applications, Renewable Energy 201;82:44-53.
[17] Zhang, L, Xu, D, Shen.G, Chen, M, Ioinovici, A, Xiaotian, W.A High Step-Up DC to DC Converter Under Alternating Phase Shift Control for Fuel Cell Power System, IEEE T on Power Electr 2015;30: 1694-1703.
[18] Kumar, M, Singh,S.N, Srivastava,S.C. Design and control of smart DC micro grid for integration of renewable energy sources. IEEE Power and Energy Society General Meeting, 2012, pp.1-7.
[19] Dupont, F.H, Rech, C, Gules, R, Pinheiro, J.R, Reduced-Order Model and Control Approach for the Boost Converter with a Voltage Multiplier Cell. IEEE T on Power Electron 2013;28:3395-3404.
[20] Rathore,A.K, Bhat,A.K.S, Nandi,S, Oruganti,R.Small signal analysis and closed loop control design of active-clamped zero-voltage switched two inductor current-fed isolated DC-DC converter. IET Power Electronics 2011;4:51-62.
[21] Middlebrook, R.D,Cuk, S. A General Unified Approach to Modeling Switching Converter Power Stages. IEEE Power Electronics specialist conference. 1976, pp.18-34.
[22] Mitchell,D.M. DC-DC Switching Regular Analysis New York:McGraw-Hill, 1988.
[23] Wong, L.K, Man, T.K. Small signal modeling of open-loop SEPIC converters. IET Power Electronics 2010;6:858-868.
[24] Venkataraman R, Bhat A.K.S.Small-signal analysis of a soft-switching, single-stage two-switch AC-DC converter. Proc. IEEE Power Electronics Specialists Conference, 2001, pp.1824-1830.
[25] Veerachary, M. Analysis of interleaved dual boost converter with integrated magnetic: signal flow graph approach. IEE Proc. Electrical Power Applications 2003;150:407-416.
[26] Mathworks: 'MATLAB User manual', 2013.
[27] PIC16F887 User manual, Microchip, Chandler, AZ, USA, 1997.